ORIGINAL RESEARCH ARTICLE

Magnesiothermic Reduction of Natural Quartz

AZAM RASOULI, KARL EDVIN HERSTAD, JAFAR SAFARIAN, and GABRIELLA TRANELL

In the current work, the metallothermic reduction of natural quartz by magnesium has been studied at 1373 K under different reaction conditions, *i.e.* quartz type, quartz particle size, Mg:SiO_2 mole ratio and reaction time. The microstructure of reaction products was studied to illustrate the reaction progression through scanning and transmission electron microscopy techniques. X-ray diffraction analysis with Rietveld phase quantification was used to calculate the change in the amount of phases at different reaction conditions. The results showed that the Mg:SiO_2 mole ratio strongly affects reaction mechanism and product characteristics such as phase content and microstructure. At lower Mg:SiO_2 mole ratios, the reaction rate is fast at the beginning and the formation of a product layer consisting of different phases such as MgO, Si, Mg_2Si, Mg_2SiO_4 and $MgSiO_3$ around quartz particles limits the Mg diffusion. This phenomenon is more noticeable for larger quartz particle sizes where Mg should diffuse longer distance towards the quartz core to react with it. At higher Mg:SiO_2 mole ratios, a significant amount of Si–Mg liquid alloy is formed during reaction where the high mobility of Mg in this liquid phase and cracking of quartz particles result in significantly higher reaction rate. Here the formation of intermediate phases is not significant and the products would be the mixture of MgO, Mg_2Si, and either Si or Mg phases.

https://doi.org/10.1007/s11663-022-02513-6

I. INTRODUCTION

WITH the rapidly increasing rate of crystalline silicon-based photovoltaic (PV) installations, the demand for sustainably produced, lower cost silicon is growing. Metallurgical Grade Silicon (MG-Si) (> 96 pct purity) is produced through carbothermic reduction of quartz in the submerged arc furnace and currently used as a precursor for high purity Si production. Main routes to purify the MG-Si to a suitably pure material (6N) for solar cell manufacturing include chemical routes (established Siemens and FBR) and metallurgical routes (including gas, slag and vacuum treatments).[1–3] In addition, direct high purity silicon production using high purity raw materials, has been considered as an alternative approach to reduce the cost of Si production. In recent years, Mg has received attention as an alternative, potentially fossil-free, reductant agent available in high purity, at a reasonable price, allowing a low temperature, exothermic reduction reaction. Although the magnesiothermic production of Si with a purity (> 99.9 wt pct) is promising, scalability of the process and low Si yield has so far limited its further development.[4–9] Further additional purification to achieve the high purities required in current high performance solar cell production would be required. As such, the overall scope of work is to produce a reduction product high in Mg_2Si, which could be directly transformed into silane gas suitable for the Siemens route.

Different studies have shown that the magnesiothermic reduction of SiO_2 may take place at low temperature, around the melting point of magnesium (923 K), where other reactants and products are in solid states. Since the vapor pressure of Mg (around 9.8×10^4 Pa) is relatively high above its melting point, it is expected that Mg in gaseous and liquid forms participate in the reaction. It has been demonstrated that diffusion of Mg to the product layer/SiO_2 interface is the rate limiting step. In other words, the reaction path is strongly dependent on the diffusivity of Mg during reaction. Theoretically, at equilibrium, 2 mol of Mg would reduce 1 mol of SiO_2 and 1 mole of Si would be produced, according to Reaction [1]. With excess Mg available during magnesiothermic reduction of SiO_2, Mg_2Si is produced according to Reaction [2]. Mg_2SiO_4 is formed as a result of Mg deficiency, according to reaction

AZAM RASOULI, KARL EDVIN HERSTAD, JAFAR SAFARIAN, and GABRIELLA TRANELL are with the Department of Materials Science and Engineering, Norwegian University of Science and Technology, 7491 Trondheim, Norway. Contact e-mail: azam.rasouli@ntnu.no

Manuscript submitted September 24, 2021; accepted March 26, 2022.

Published online: 19 April 2022

[3].[7,10–19] However, there is little information in the literature on how reaction conditions affect formation of different phases quantitatively. Moreover, high purity natural quartz, considering its abundance and low price, is an attractive raw material to produce Si with higher purity than MG-Si, especially with low content in boron (B) and phosphorus (P) that are challenging to remove metallurgically.[2] In this initial study, we hence aim at providing a better understanding of the reaction paths in magnesiothermic reduction of high purity natural quartz by investigating different parameters including Mg:SiO_2 mole ratio, time, quartz particle size and quartz type.

$$SiO_2 + 2Mg = 2MgO + Si \quad \Delta G^0_{1373} = -243.4\ \text{kJ} \quad [1]$$

$$SiO_2 + 4Mg = 2MgO + Mg_2Si \quad \Delta G^0_{1373} = -272.1\ \text{kJ} \quad [2]$$

$$SiO_2 + Mg = 0.5Mg_2SiO_4 + 0.5Si \quad \Delta G^0_{1373} = -146.4\ \text{kJ} \quad [3]$$

II. EXPERIMENTAL MATERIALS AND PROCEDURE

A. *Materials*

The reduction reaction was carried out using three types of natural quartz and metallic magnesium as raw materials. As can be seen in Table I, the quartz types A and F are highly pure and type D has a small amount of impurity elements. Moreover, quartz types A and F are hydrothermal metamorphic type while quartz type D is a quartzite.

The quartz lumps were crushed first with a jaw crusher and next in a tungsten carbide ring mill to smaller particles. After crushing, quartz particles were screened to produce three different particle size ranges using sieves with 45 to 53 μm, 500 to 600 μm and 3.15 to 3.35 mm opening size. After sieving, the particle size distributions of the resulting quartz particles were measured by a laser scattering particle size distribution analyzer, Partica LA-960. The median quartz particle sizes with their standard deviations are reported in Table II. As a reductant agent, metallic Mg in the form of turnings were supplied by Alfa Aesar (purity of ≥ 99.8 wt pct and in the size range of ≤ 3.2 mm).

B. *Experimental Set-Up*

Reduction experiments were carried out in a gas-tight stainless-steel reactor. For each experiment, approximately 1 g of quartz and a selected amount of Mg turnings were weighed and added to the high purity Al_2O_3 crucible to obtain the desired Mg:SiO_2 mole ratios indicated in Table II. At each mole ratios, about 10 wt pct of more Mg was used due to possible of Mg loss. The reactor was subsequently tightened firmly inside the glovebox with Ar atmosphere. To be able to monitor temperature during the reaction, a thermowell for accommodating a thermocouple was designed in the lid of the reactor. The assembly was placed on a platform rod at the bottom of a graphite tube furnace that has two thermocouples. The thermocouple on the side of the furnace was controlling the furnace temperature, while the thermocouple from the top of the furnace monitored the reactor temperature. After reaching the set temperature of 1373 K, the reactor was inserted into the hot zone of the furnace by pushing the rod assembly upwards. The furnace setup and reactor are shown in Figure 1. All experiments were conducted under the flow of Ar gas. After desired reaction time outlined in Table II, the reactor was removed by pulling the rod assembly into the cold zone of the furnace.

C. *Product Characterization*

The product phases after reduction reaction were identified by powder X-ray diffraction test using Bruker D8 Focus with CuKα radiation (wavelength of 1.54 Å) and LynxEye™ SuperSpeed Detector. The X-ray diffraction tests were performed from 5 to 115 deg diffraction angle and using a step size of 0.016 deg. Quantitative phase analysis was done based on the Rietveld method by the TOPAS 5 software.[21] Furthermore, a microstructure examination of the product was performed by Field Emission Scanning Electron Microscopy (Zeiss Ultra FESEM) equipped with XFlash® 4010 Detector supplied by Bruker Corporation for Energy-Dispersive X-ray Spectroscopy (EDS). To study the microstructure more deeply, two lamellas were prepared by focused ion beam (FIB) using a Helios G4 UX dual-beam instrument. Transmission Electron Microscopy examination was done by double Cs aberration corrected cold FEG JEOL 200FC equipped with Centurio detector for Energy-Dispersive X-ray Spectroscopy (EDS) and a GIF Quantum ER for Electron Energy Loss Spectroscopy (EELS).

III. RESULTS AND DISCUSSION

A. *Effect of Mg:SiO_2 Mole Ratio*

To study the effect of amount of Mg available during reaction on the product phases, quartz particles were reacted with Mg at Mg:SiO_2 mole ratios of 1, 2, 3 and 4. The selection of a wide range of molar ratios was to evaluate well the effect of reactant portions on the type and amount of products. The X-ray diffraction patterns for the reacted 704 μm quartz particle size of type A* and different Mg:SiO_2 mole ratios are illustrated in Figure 2 (X-ray diffraction patterns of other quartz particle sizes and Mg:SiO_2 mole ratios can be found in Figures S-1 through S-4 refer to Electronic Supplementary Material). The phase distribution obtained from

*The quartz type studied in the sections A and B is type A.

Table I. Chemical Composition of Three Types of Natural Quartz as Raw Materials Obtained from Inductively Coupled Plasma-Optical Emission Spectrometry (ICP-OES) (the Analysis was Performed by Jusnes[20])

Quartz Type	Al (ppm)	Fe (ppm)	K (ppm)	Mg (ppm)	Na (ppm)	Ca (ppm)	Ti (ppm)	Mn (ppm)	P (ppm)	SiO_2 (Wt Pct)
A	106	20	23	9	10	3	4.2	0.3	< 2.6	99.982
D	2603	2443	626	42	28	33	145.8	< 0.1	25.6	99.405
F	90	20	40	10	50	10	4.1	1.2	< 2.6	99.977

Table II. The Studied Reduction Reaction Parameters

Parameters	Parameter Settings
Median Quartz Particle Size (μm)	57 ± 25, 704 ± 175, 3360 ± 780
Reaction Time (Min)	10, 20, 40, 60, 120
Mg:SiO_2 Mole Ratio	1, 2, 3, 4*

*Regarding 10 wt pct more Mg, the exact mole ratios are 1.1, 2.2, 3.3 and 4.4.

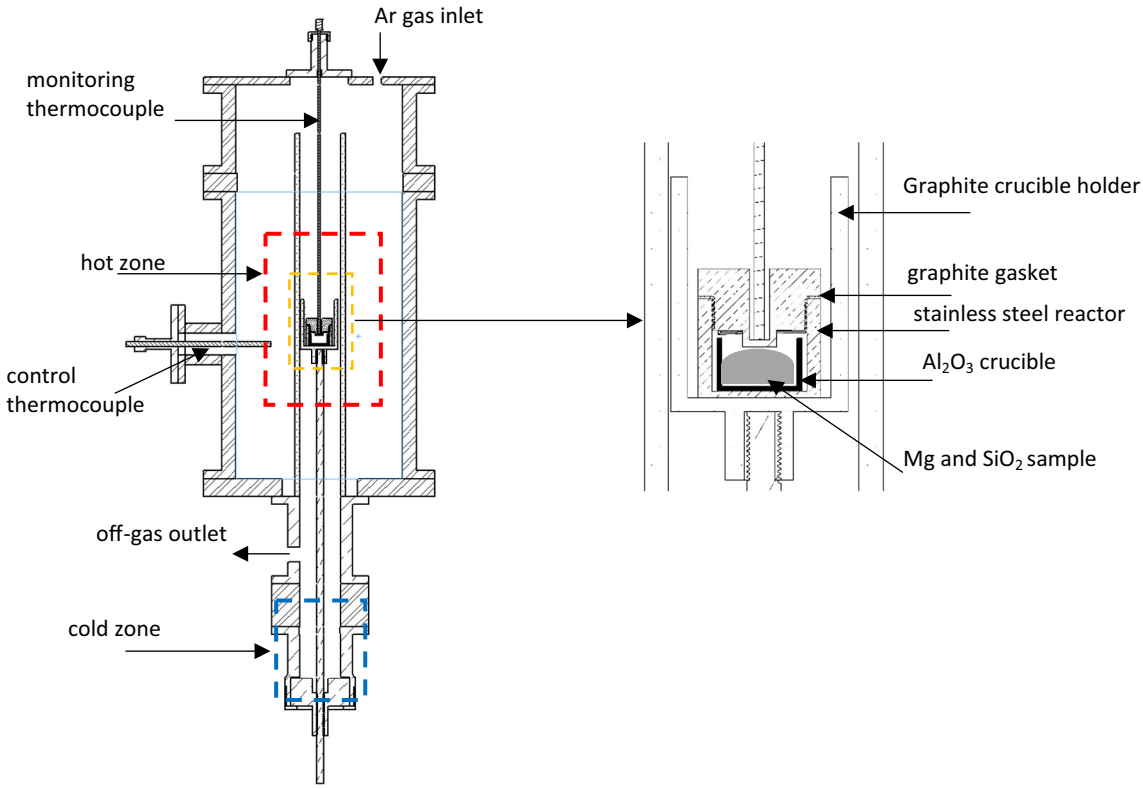

Fig. 1—Schematic of set-up used to conduct reduction reactions.

Rietveld analysis of the reacted samples and the phase distribution at equilibrium condition (calculated by FactSage 7.3) are compared in Table III. At a mole ratio of 1, the quartz is partially reduced to Si and while the Si content broadly agrees with equilibrium calculations, only a small amount of Mg_2SiO_4 phase was measured compared to the calculated one. A significant fraction of unreduced SiO_2 and MgO were, however, measured in the product. By increasing the Mg:SiO_2 mole ratio to 2 and 3, equilibrium calculations yield varying mixtures of MgO, Si and Mg_2Si products. The experimental result at a mole ratio of 2 shows that most of the quartz was reduced to Si and with excess available Mg in the Mg_2Si phase. Compared with the mole ratio of 1, very little SiO_2 and Mg_2SiO_4 phases were detected for the mole ratio of 2, which agrees with equilibrium calculations. At a mole ratio of 3, all quartz was reduced and consequently more Mg_2Si phase was detected. At a

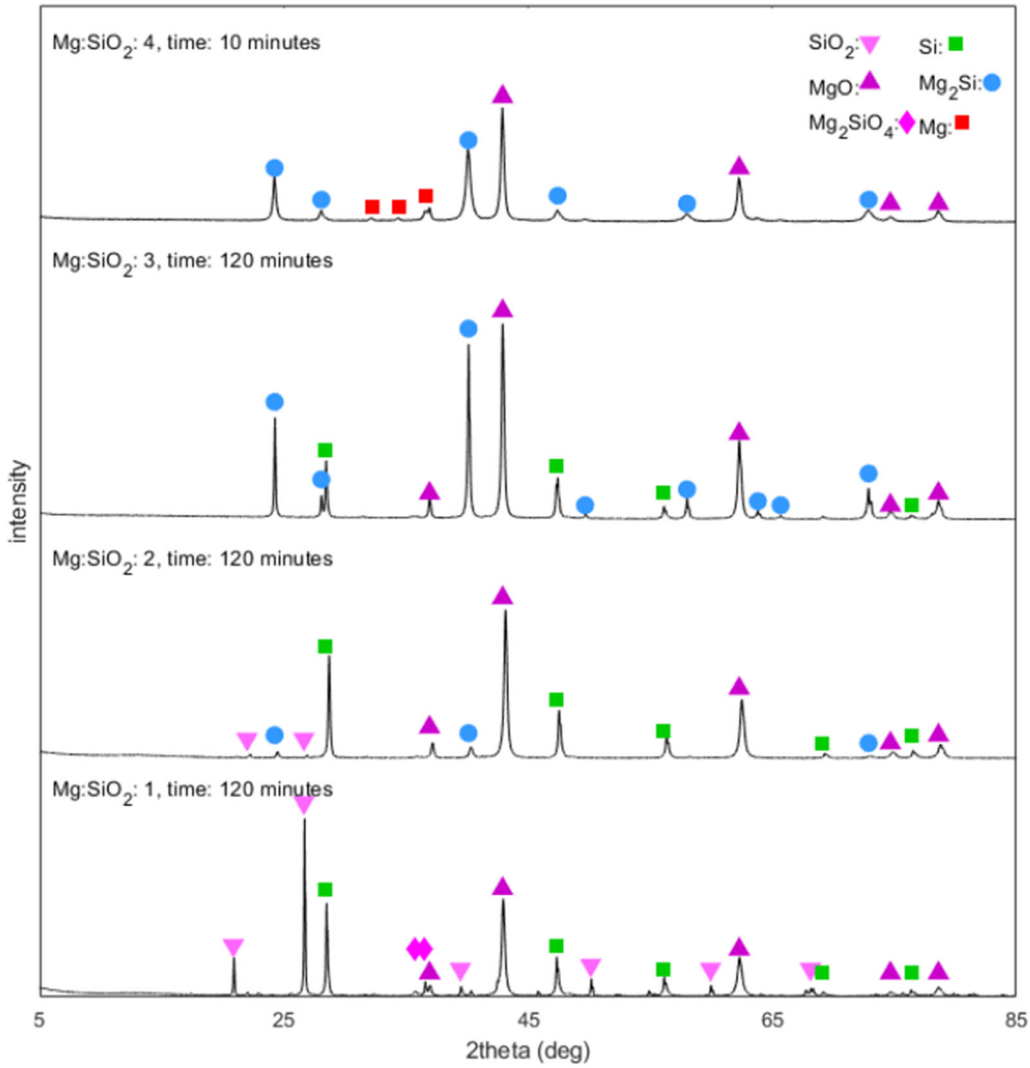

Fig. 2—X-ray diffraction patterns of 704 μm quartz particle size of type A samples at different Mg:SiO_2 mole ratios.

mole ratio of 4, enough Mg is available to contain all Si in the form of Mg_2Si in addition to excess unreacted Mg. In summary; except for the lower amount of Mg_2SiO_4 in the reaction product for the mole ratio of 1, there is generally a good agreement between calculated phase distribution at equilibrium and those established by quantitative phase analysis by the Rietveld method. This indicates that conditions in the samples with higher Mg:SiO_2 mole ratios are closer to equilibrium than ones with lower Mg:SiO_2 mole ratios.

The backscattered electron images with X-ray mapping of Si, Mg and O elements of the samples discussed above are given in Figure 3. In Figure 3(a), an initial quartz particle transformed into a four-layer product is illustrated for a Mg:SiO_2 mole ratio of 1. In the core, there is unreacted quartz that is surrounded by a thin layer (the composition of this layer will be discussed in section D). The next layer is composed of an integrated mixture of MgO and Si phases. The outer layer of the particle consists of porous MgO with some Si seen as bright areas. At a mole ratio of 2, the quartz particle displays a similar four-layer structure, shown in Figure 3(e). However, smaller unreacted core and more Si as thin bright veins (in 2D) in the outer MgO layer, are observed compared to the sample in Figure 3(a). X-ray mapping of Si, Mg and O elements in Figures 3(b) through (d) and Figures 3(f) through (h) for mole ratios of 1 and 2, respectively, demonstrate that magnesiothermic reduction of SiO_2 can be best described by the shrinking unreacted core model where Mg diffuses into the initial quartz particles to react with it. The product of the reaction between SiO_2 and Mg forms a layer around unreacted SiO_2 core. To progress reaction further, Mg has to diffuse through the product layer to reach the unreacted SiO_2 in the core of the particle.[22]

The microstructure of the reaction product is completely different when the Mg:SiO_2 mole ratio is 3 or 4, as shown in Figures 3(i) and (m), respectively. In these figures, the matrix is the Mg_2Si product phase enclosing two other phases. The secondary phase in the matrix is Si for the mole ratio of 3 and unreacted Mg for the mole ratio of 4. The dark particles represent the MgO phase that initially were quartz particles. It is clearly seen that original particles have fractured into smaller particles

Table III. Phase Distribution at Equilibrium Condition and Experiments for 704 μm Quartz Particle Size of Type A Samples at Different Mg:SiO_2 Mole Ratios

Conditions	Mg:SiO_2 Mole Ratio	Amount of Phases (Wt Pct)					
		MgO	Si	Mg_2Si	SiO_2	Mg_2SiO_4	Mg
Equilibrium Condition	1	8.2	17.7	—	—	74.2	—
	2	71.0	22.3	6.8	—	—	—
	3	58.3	8.0	33.7	—	—	—
	4	48.3	—	45.9	—	—	5.8
Experiments	1	52.9	15.6	—	25.0	6.5	—
	2	74.9	19.3	4.4	1.0	0.3	—
	3	61.5	7.4	31.0	—	—	—
	4	56.6	—	40.7	—	—	2.8

Equilibrium condition was calculated based on Mg:SiO_2 mole ratios of 1, 2, 3 and 4 plus 10 wt pct excess Mg.

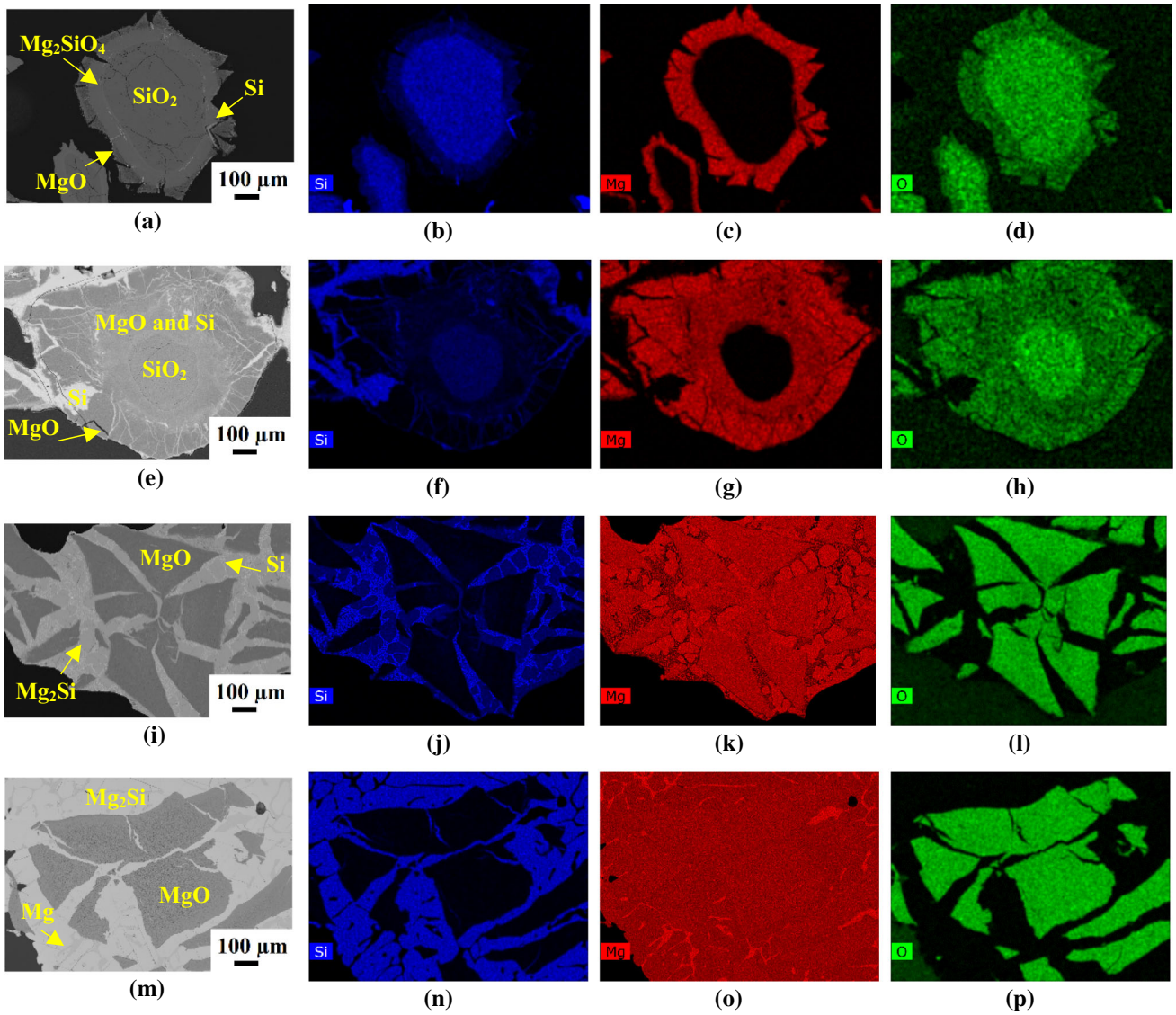

Fig. 3—(*a*) Backscattered electron image of sample with a Mg:SiO_2 mole ratio of 1 and 120 min reaction time, (*b*) to (*d*) X-ray mapping of Si, Mg and O elements of the sample in figure (a), (*e*) backscattered electron image of sample with a Mg:SiO_2 mole ratio of 2 and 120 min reaction time, (*f*) to (*h*) X-ray mapping of Si, Mg and O elements of the sample in figure (e), (*i*) backscattered electron image of sample with a Mg:SiO_2 mole ratio of 3 and 120 min reaction time, (*j*) to (*l*) X-ray mapping of Si, Mg and O elements of the sample in figure (i), (*m*) backscattered electron image of sample with a Mg:SiO_2 mole ratio of 4 and 10 min reaction time, (*n*) to (*p*) X-ray mapping of Si, Mg and O elements of the sample in figure (m), initial quartz particle size is 704 μm for all samples.

during reaction. The distribution of phases at equilibrium, listed in Table S-I, verifies that a large amount of Si–Mg liquid is formed at the reaction temperature of 1373 K. The formation of the liquid phase facilitates penetration of Mg in the liquid phase into the cracks of the quartz particles and enhances the reaction rate. Cracking of quartz particles is also observed at mole ratios of 1 and 2 (Figures 3(a) and (e)), but there is not enough liquid phase to penetrate into the cracks during the reaction at these mole ratios. During cooling, first Mg_2Si precipitates from liquid. At the mole ratio of 3, the remaining liquid phase solidifies as Mg_2Si and Si phases *via* the eutectic reaction at 1218 K, while at the mole ratio of 4, the liquid phase converts to Mg_2Si and Mg at the 912 K eutectic point, as shown in Figure S-5. For lower reaction temperatures (773 K to 973 K), periodic layered structures composed of alternating layers of MgO and Mg_2Si, have been previously reported.[11,19,23,24] In more recent work, it was shown that each sublayer may contain one phase as major phase and the other one as minor phase.[23] This periodic layered structure was attributed to the high mobility of Mg atoms *vs* low diffusion rate of Si atoms. In other words, Si atoms formed by reduction reaction diffuses outwards and accumulates outside the MgO layer as a Mg_2Si layer. The MgO and Mg_2Si layers grow until the MgO layer creates a barrier against Si diffusion. At this point, new sublayers of MgO and Mg_2Si would be formed. In the current work, however, a different structure has been observed as the high temperature of reaction leads to Mg–Si liquid. It also worth mentioning that this periodic layered structure is only observed when Mg_2Si is one of the main products of the reduction reaction.

B. *Effect of Reaction Time and Quartz Particle Size*

It is known from prior work that the rate of magnesiothermic reduction of SiO_2 is controlled by the rate of Mg diffusion. As reaction time and diffusion distance are two important parameters in diffusion controlled processes, the magnesiothermic reduction experiments were performed on different quartz particle sizes and varying reaction time. The backscattered

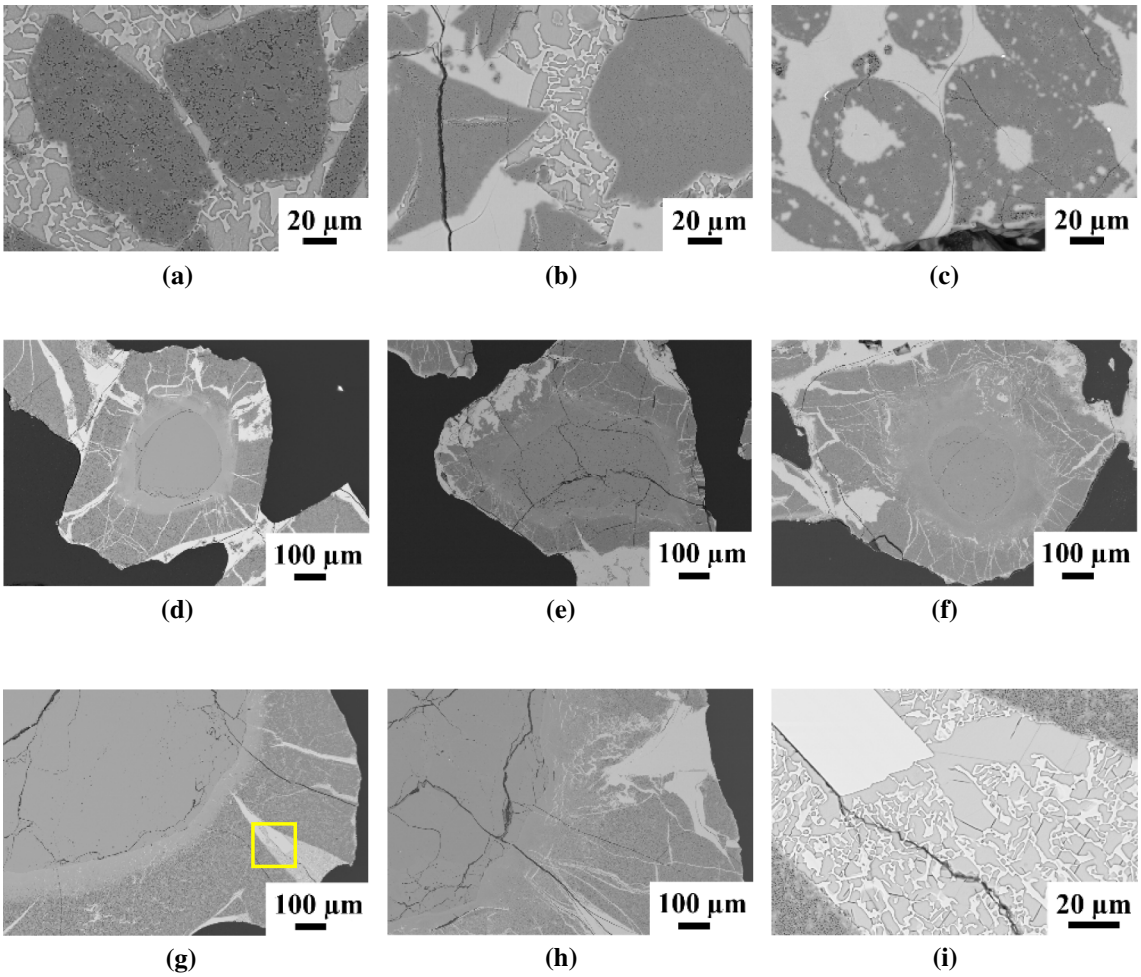

Fig. 4—Backscattered electron image of samples with a Mg:SiO_2 mole ratio of 2 with different quartz particle sizes and reaction time, (*a*) to (*c*) 57 μm quartz particle size and 10, 20 and 120 min reaction time, respectively, (*d*) to (*f*) 704 μm quartz particle size and 10, 20 and 120 min reaction time, respectively. (*g*) and (*h*) 3360 μm quartz particle size and 10 and 120 min reaction time, respectively, (*i*) higher magnification of area shown in the yellow square in figure (g).

electron images of these samples against reaction time for a mole ratio of 2 are given in Figure 4. For all three quartz particle sizes, a noticeable amount of Mg_2Si is observed after a short reaction time at the particle periphery. Moving towards the particle core, elemental Si is found close to the reaction front. With increasing reaction time, the Mg_2Si phase is converted to Si as it is not thermodynamically stable under these reaction conditions. This observation is illustrated as a change in Mg_2Si phase content against reaction time, shown in Figure 5(a) for mole ratios of 1 and 2. With, for example, the 704 μm quartz particle size and a mole ratio of 2, the Mg_2Si content decreases from about 8.9 to 4.4 wt pct with increasing reaction time from 10 to 120 minutes. At the beginning of the reaction, Mg melts, evaporates, and rapidly reduces quartz at the particle periphery. The Si produced and the inwards diffusing Mg vapor may form a liquid phase according to the Si-Mg binary phase diagram, Figure S-5. With increasing reaction time, Mg in the liquid phase diffuses into the particle to further reduce quartz. Consequently, there would be less Mg_2Si with longer reaction time. At each mole ratio, the highest amount of Mg_2Si is obtained for the largest quartz particle size (6.9 and 14.7 wt pct for mole ratios of 1 and 2, respectively, and 3360 μm quartz particle size), which further confirms that the Mg_2Si formation is related to the limitation in Mg diffusion. As seen in Figures 4(d) through (f), it is apparent that the size of the unreacted quartz core is

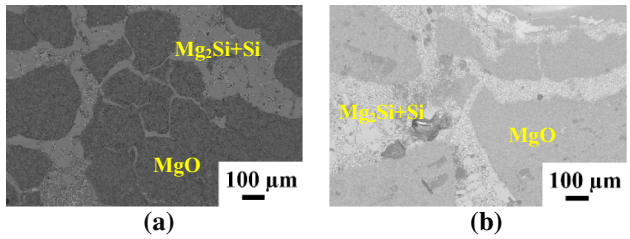

Fig. 6—Backscattered electron image of quartz type D (*a*) and quartz type F (*b*) at a mole ratio of 3, 704 μm quartz particle size and 10 minutes reaction time.

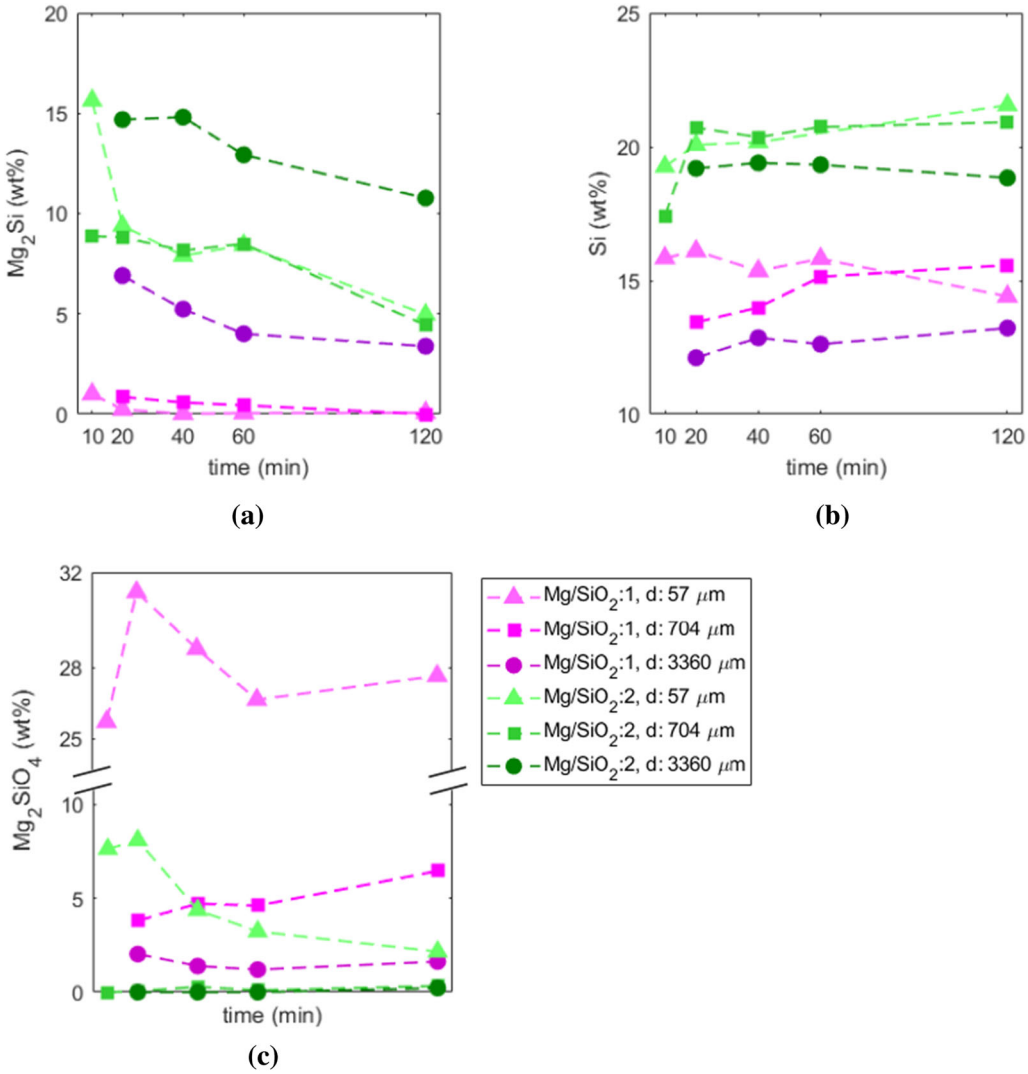

Fig. 5—The change in the amount of Mg_2Si (*a*), Si (*b*) and Mg_2SiO_4 (*c*) phases against reaction time at Mg:SiO_2 mole ratios of 1 and 2.

decreasing with time for 704 μm quartz particle size. For higher mole ratios of 3 and 4, there is no significant change in the microstructure of samples with increasing reaction time, as shown in Figures S-6 and S-7, respectively.

The comparison of total formed Si (sum of produced Si in Si and Mg_2Si phases), Figure 5(b), reveals that Si was formed already after 10 minutes reaction time for all conditions (two mole ratios and different particle sizes) and increases with increasing reaction time. After 120 minutes reaction time, the Si content in the two smaller size fractions (57 and 704 μm) has reached a stable, equivalent equilibrium level, while the largest particles (3360 μm) have a lower Si content indicating incomplete reduction reaction even after 120 minutes reaction time. As summarized in Table III, the equilibrium content of Mg_2SiO_4 is 74.2 wt pct at the mole ratio of 1. Figure 5(c) shows that the maximum measured Mg_2SiO_4 content is less than half of this amount, around 31.2 wt pct for the 57 μm quartz particle size. The Mg_2SiO_4 content in the finest particle size initially increases for up to 20 minutes reaction time, thereafter, decreasing for the sample held up to 60 minutes and subsequently stabilizing at slightly higher contents. For the 704 μm quartz particle size, maximum Mg_2SiO_4 content is around 6.5 wt pct, while for 3360 μm quartz particle size is only around 2 wt pct after 120 minutes reaction time. It is clear from these results that approaching the equilibrium content of Mg_2SiO_4 is kinetically limited by the slow diffusion rate of elements in solid state. Hence, a higher interfacial area between the unreacted quartz and the product phase would result in more Mg_2SiO_4 formation for smaller particle sizes. At a mole ratio of 2, the Mg_2SiO_4 phase is only noticeable for the 57 μm quartz particle size. Mg_2SiO_4 was formed initially and is subsequently decreasing rapidly with time. As discussed in section D, the Mg_2SiO_4 phase is formed during the reduction of quartz by Mg as an intermediate phase at a mole ratio of 2.

C. *Effect of Quartz Type*

The properties of three quartz types have been thoroughly studied elsewhere.[20] In addition to differences in impurity elements content, these quartz types vary in grain size, thermal disintegration behavior, fluid inclusions and pre-existing cracks. However, the backscattered electron images for different quartz types, comparison Figures 3(i), 6(a) and 6(b), demonstrate no significant difference in the reduction behavior between different quartz types at a $Mg:SiO_2$ mole ratio of 3.

D. *Detailed Analysis of the Mechanism of the Reaction at Lower $Mg:SiO_2$ Mole Ratio*

To investigate the reaction mechanism in more detail, High-Angle Annular Dark-Field (HAADF) images from different areas together with simultaneous Electron Energy Loss Spectroscopy (EELS) and Energy Dispersive X-ray Spectroscopy (EDS) elemental mapping of the sample with a $Mg:SiO_2$ mole ratio of 2 and 704 μm quartz particle size was carried out that typical results are presented in Figure 7. The exact position of the two prepared TEM lamellas can be found in Figure S-8. To discuss the different layers, we start from the interface between unreacted quartz core and product in Figure 7(a). The figure reveals that the thin layer around the unreacted core (indicated in section A) is composed of two layers. The average chemical compositions of these two layers are given in the ternary phase diagram of Mg–Si–O in Figure 8. The layer adjacent to the quartz core (layer (i)) contains Si and a Mg–Si–O phase with a

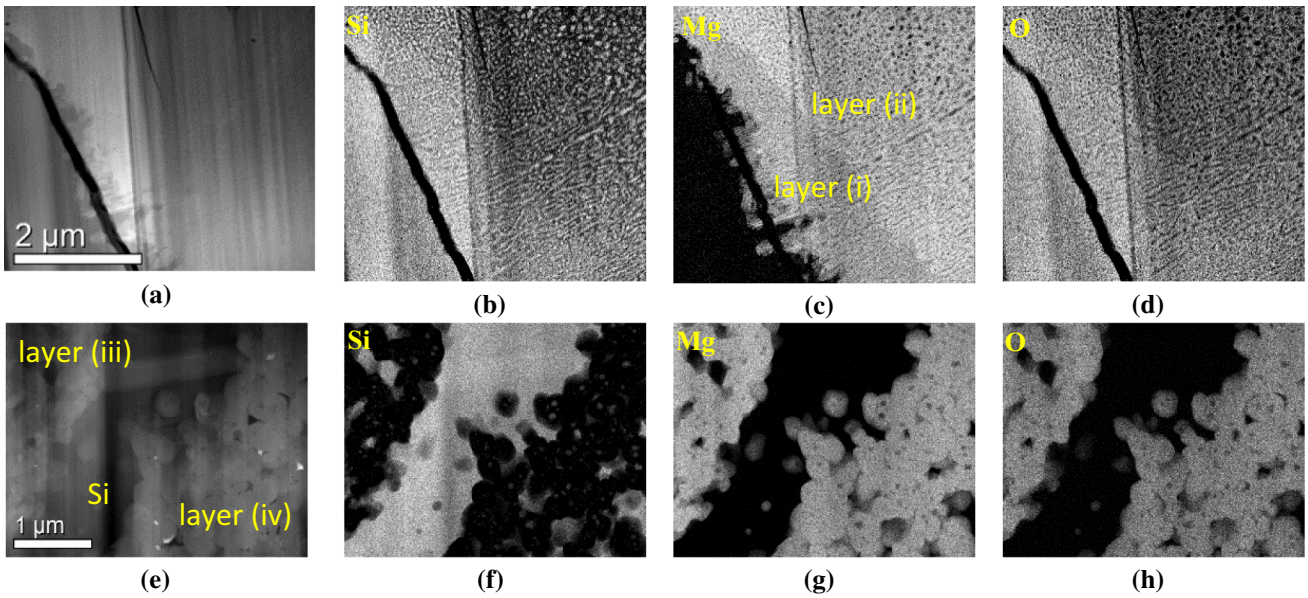

Fig. 7—HAADF STEM image and STEM-EELS-EDS element mapping of Si, Mg and O of the sample with a $Mg:SiO_2$ mole ratio of 2 and 704 μm quartz particle size, (*a*) interface between unreacted SiO_2 core and product, (*b*) to (*d*) element mapping, (*e*) interface between layer (iii) and layer (iv) (outer layer), (*f*) to (*h*) element mapping.

stoichiometry close to $MgSiO_3$. The second layer (layer (ii)) around quartz core contains some MgO in addition to Si and a Mg–Si–O phase. In this layer, the Mg–Si–O stoichiometry is close to Mg_2SiO_4. The formation of these layers is well described by the Mg–Si–O ternary phase diagram determining which phases can co-exist at equilibrium. The HAADF image from the interface between layer (iii) and outer layer (layer (iv)) exhibits in Figure 7(e). The average chemical composition shows that layer (iii) contains MgO and Si phase while layer (iv) contains more MgO phase with less Si content indicating separation of Si, Figure 8. There are also some Mg_2Si and Mg phases in layer (iii) and layer (iv) that indicates the diffusion of Mg through the product layer.

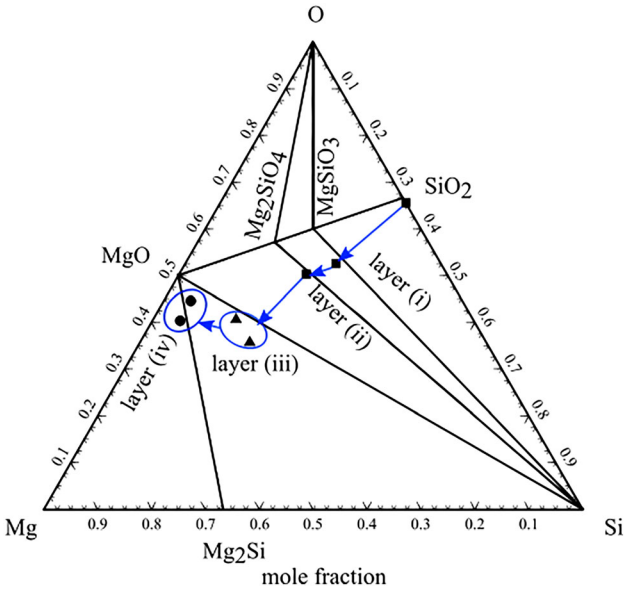

Fig. 8—Ternary phase diagram of Si–Mg–O calculated by FactSage 7.1.

Based on these observations, the steps of reduction reaction are illustrated in Figure 9. The reduction of SiO_2 happens through series of intermediate reactions. Firstly, SiO_2 is reduced to a mixture of $MgSiO_3$ and Si shown as layer (i) according to reaction [4]. By diffusion of more Mg, $MgSiO_3$ reacts with Mg, according to reaction [5], to produce a Mg_2SiO_4 and Si mixture that forms layer (ii) (time t_1 in Figure 9). Finally, reduction of Mg_2SiO_4 by Mg to a mixture of MgO and Si takes place according to reaction [6] (time t_2 in Figure 9). The just- formed MgO and Si mixture has an integrated structure but Si will subsequently separate from the mixture with time and accumulate either at the periphery of the particles or as thin veins (in 2D image) in the MgO matrix due to the low wettability of MgO by Si.[25] Simultaneously, Mg may combine with the produced Si that is seen as a Mg_2Si phase precipitating during cooling. Hence, the propagation of the reaction front into the quartz core takes place through these intermediate reactions rather than directly through reaction [1] until SiO_2 converts completely to products (time t_3 in Figure 9). In other words, the reaction proceeds *via* the mass transport of Mg through both the co-existing intermediate phases of Mg_2SiO_4 and $MgSiO_3$. As mentioned previously, the reaction rate is fast until the product layer of MgO and Si introduces a barrier against Mg diffusion. The formation of the intermediate phases between SiO_2 and products was also reported in other studies.[11,24] In the study by Kodentsov *et al.*[21] on the interaction between monocrystalline SiO_2 and a Mg diffusion couple at temperatures of 500 °C and 550 °C, MgO was formed in a layer adjacent to SiO_2 in a short reaction time experiment. The formation of $MgSiO_3$ and Mg_2SiO_4 was seen in longer reaction time

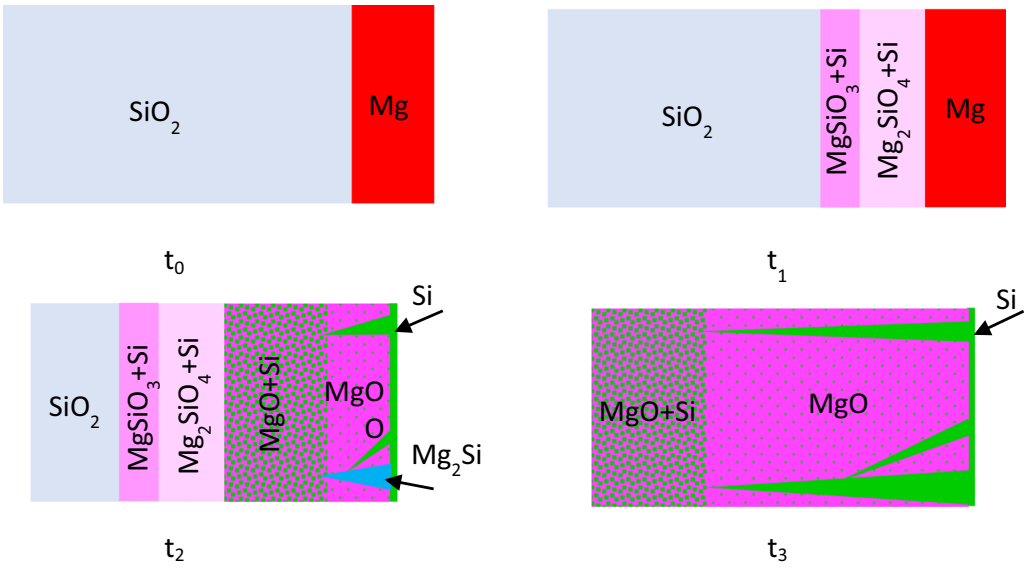

Fig. 9—Schematic of reaction steps with formation of different layers around untreated quartz core from $t_0 = 0$ to t_3 that t_3 is the reaction time for complete reduction of quartz ($t_0 < t_1 < t_2 < t_3$).

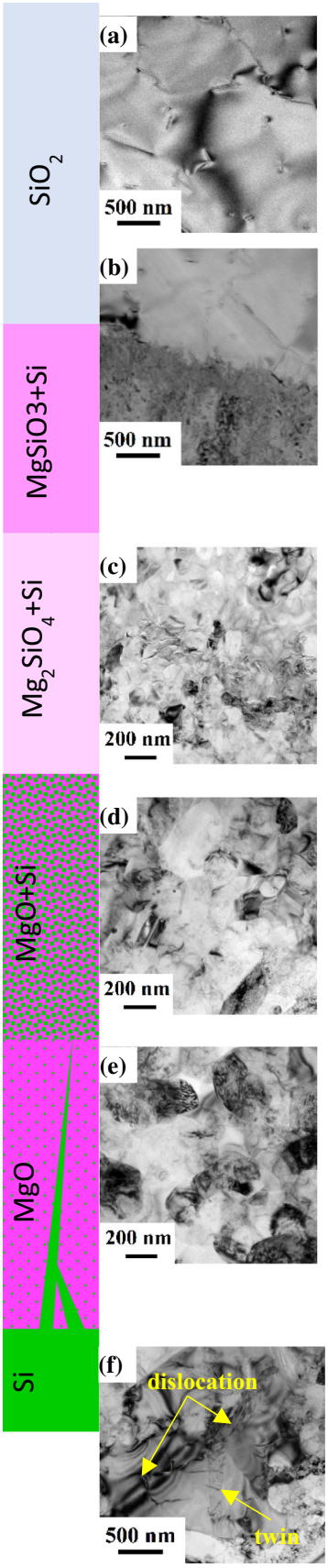

◀Fig. 10—Schematic and BF images of different layers formed during reduction reaction of the sample with a Mg:SiO_2 mole ratio of 2 and 704 μm quartz particle size, (*a*) unreacted quartz core, (*b*) the interface between unreacted quartz and layer (i), (*c*) layer (ii) with Mg_2SiO_4 and Si phases, (*d*) layer (iii) with MgO and Si phases, (*e*) layer (iv), (*f*) Si grain in layer (iv).

experiments, and it was concluded to be due to establishment of equilibrium in the diffusion zone in longer reaction time.

The bright field images from different areas of the quartz with a Mg:SiO_2 mole ratio of 2 and 704 μm particle size are seen in Figure 10. The natural quartz material is composed of large grains in the order of a few micrometers that strain contrast from dislocations inside grains is seen in Figure 10(a). Figure 10(b) shows the penetration of Mg into SiO_2. Images in Figures 10(c), (d) and (e) show a nano-grained structure as well as a high density of defects. Decreasing grain size from a few micrometers to a few hundred nanometers indicates that there must be high number of nucleation sites during the reduction reaction. Moreover, a higher density of defects shown in Figure 10(e) compared to Figure 10(d) is attributed to the diffusion of Si away, leaving a porous MgO structure. Finally, the presence of dislocations and twin band in the Si, Figure 10(f), confirms that Si is formed from a liquid phase.

$$2Mg + 3SiO_2 = 2MgSiO_3 + Si \quad \Delta G^0_{1373} = -293.3 \text{ kJ} \quad [4]$$

$$2Mg + 4MgSiO_3 = 3Mg_2SiO_4 + Si \quad \Delta G^0_{1373\,K} = -287.6 \text{ kJ} \quad [5]$$

$$2Mg + Mg_2SiO_4 = 4MgO + Si \quad \Delta G^0_{1373\,K} = -173.6 \text{ kJ} \quad [6]$$

IV. CONCLUSIONS

In the current work, mechanisms and reactions governing the rate and products of magnesiothermic reduction of natural quartz particles were investigated. The conclusions of the study are:

- The reaction is strongly dependent on the amount of Mg available in terms of both reaction mechanism and reaction rate.
- At Mg:SiO_2 mole ratios of 1 and 2, MgO and Si are the main products. After initial formation of Si, the reaction rate decreases due to the low diffusion rate of Mg through the product layer. While the reaction occurs through the formation of intermediate phases at the reaction front ($MgSiO_3$ and Mg_2SiO_4 phases) around unreacted quartz particle core, Mg_2Si is formed in outer areas of particles with higher concentrations of Mg. The observed sequence of phases

from the unreacted core to the surface of a particle is $SiO_2/MgSiO_3/Mg_2SiO_4/MgO–Si/Si–Mg_2Si–MgO$.
- At Mg:SiO_2 mole ratios of 1 and 2, smaller particle sizes show higher reaction rate; fastest and complete reaction for 57 μm quartz particle size and slowest for 3360 μm quartz particle size with some unreacted quartz at the examined conditions.
- At Mg:SiO_2 mole ratios of 3 and 4, the formation of a high amount of liquid and cracking of quartz particles accelerate the reduction reaction and also the largest 3360 μm quartz particles are reduced rapidly due to the higher Mg mobility/diffusion. The final products are composed of mixtures of MgO–Mg_2Si–Si and MgO–Mg_2Si–Mg for mole ratios of 3 and 4, respectively.
- Different natural quartz types display the same reduction reaction mechanisms at high temperature (1373 K) and high Mg:SiO_2 mole ratio.

ACKNOWLEDGMENT

This work was performed at NTNU within the Research Centre for Sustainable Solar Cell Technology (FME SuSolTech, Project Number 257639), co-sponsored by the Norwegian Research Council and industry partners.

CONFLICT OF INTEREST

On behalf of all authors, the corresponding author states that there is no conflict of interest.

FUNDING

Open access funding provided by NTNU Norwegian University of Science and Technology (incl St. Olavs Hospital - Trondheim University Hospital).

OPEN ACCESS

SUPPLEMENTARY INFORMATION

The online version contains supplementary material available at https://doi.org/10.1007/s11663-022-02513-6.

REFERENCES

1. A. Schei, J.K. Tuset, and H. Tveit: *Production of High Silicon Alloys*, TAPIR forlag, Trondheim, 1998.
2. J. Safarian, G. Tranell, and M. Tangstad: *Energy Procedia.*, 2012, vol. 20, pp. 88–97.
3. J. Safarian and M. Tangstad: *Metall. Mater. Trans. B.*, 2012, vol. 43B, pp. 1427–45.
4. W. James A. Amick, Princeton, N.J.; John W. Milewski, Los Alamos, N. Mex.; Franklin J.Wright and N.J.: *United States Pat. 4214920*.
5. R. Kvande: in *Silicon for the Chemical and Solar Industry X*. H.A. Øye, H. Brekken, and L. Nygaard, eds., Tapir Uttrikk, Ålesund-Geiranger, 2010, pp. 191–201.
6. H.D. Banerjee, S. Sen, and H.N. Acharya: *Mater. Sci. Eng.*, 1982, vol. 52, pp. 173–79.
7. M. Barati, S. Sarder, A. Mclean, and R. Roy: *J. Non. Cryst. Solids.*, 2011, vol. 357, pp. 18–23.
8. K.K. Larbi, R. Roy, M. Barati, and V.I. Lakshmanan: *Biomass Convers. Biorefinery.*, 2012, vol. 2, pp. 149–57.
9. K.C. Nandi, D. Mukherjee, A.K. Biswas, and H.N. Acharya: *Sol. Energy Mater.*, 1991, vol. 22, pp. 161–67.
10. K.H. Sandhage, M.B. Dickerson, P.M. Huseman, M.A. Caranna, J.D. Clifton, T.A. Bull, T.J. Heibel, W.R. Overton, and M.E.A. Schoenwaelder: *Adv. Mater.*, 2002, vol. 14, pp. 429–33.
11. Y.C. Chen, J. Xu, X.H. Fan, X.F. Zhang, L. Han, D.Y. Lin, Q.H. Li, and C. Uher: *Intermetallics.*, 2009, vol. 17, pp. 920–26.
12. J.K. Yoo, J. Kim, M.J. Choi, Y.U. Park, J. Hong, K.M. Baek, K. Kang, and Y.S. Jung: *Adv. Energy Mater.*, 2014, vol. 4, pp. 1–9.
13. Z. Bao, M.R. Weatherspoon, S. Shian, Y. Cai, P.D. Graham, S.M. Allan, G. Ahmad, M.B. Dickerson, B.C. Church, Z. Kang, H.W.A. Iii, C.J. Summers, M. Liu, and K.H. Sandhage: *Nature.*, 2007, vol. 446, pp. 172–75.
14. J.R. Wynnyckyj and D. Bhogeswara Rao: *High Temp. Sci.*, 1976, vol. 8, pp. 203–17.
15. I.A. Ødegård, J. Romann, A. Fossdal, A. Røyset, and G. Tranell: *J. Mater. Chem. A.*, 2014, vol. 2, pp. 16410–15.
16. J.E. Entwistle, G. Beaucage, and S.V. Patwardhan: *J. Mater. Chem. A.*, 2020, vol. 8, pp. 4938–49.
17. J. Entwistle and A. Rennie: *J. Mater. Chem. A.*, 2018, vol. 6, pp. 18344–56.
18. J. Liang, X. Li, Z. Hou, W. Zhang, Y. Zhu, and Y. Qian: *ACS Nano.*, 2016, vol. 10, pp. 2295–304.
19. I. Gutman, I. Gotman, and M. Shapiro: *Acta Mater.*, 2006, vol. 54, pp. 4677–84.
20. K.F. Jusnes: *Norwegian University of Science and Technology*, 2020.
21. R.A. Young, ed.: *The Rietveld Method*, Oxford University Press Inc., New York, 1993.
22. J. Szekely, J.W. Evans, and H.Y. Sohn, eds.: *Gas–Solid Reactions*, Academic Press, New York, 1976.
23. L. Shi, P. Shen, D. Zhang, E. Dong, and Q. Jiang: *Appl. Surf. Sci.*, 2013, vol. 274, pp. 124–30.
24. A. Kodentsov, A. Wierzbicka-miernik, L. Litynska-dobrzynska, P. Czaja, and J. Wojewoda-budka: *Intermetallics.*, 2019, vol. 114, pp. 1–10.
25. H. Iyer, L. TafaghodiKhajavi, D. Durlik, K. Danaei, and M. Barati: *Silicon.*, 2018, vol. 10, pp. 2219–26.